Comparison of MEO, LEO, and terrestrial IoT configurations in terms of GDOP and achievable positioning accuracies

Ruben Morales Ferre, *Student Member, IEEE and* Elena Simona Lohan, *Senior Member, IEEE*

Abstract—Complementary solutions to the Medium Earth Orbit (MEO) Global Navigation Satellite Systems (GNSS) are more and more in demand to be able to achieve seamless positioning worldwide, in outdoor as well as in indoor scenarios, and to cope with increased interference threats in GNSS bands. Two of such complementary systems can rely on the emerging Low Earth Orbit (LEO) constellations and on the terrestrial long-range Internet of Things (IoT) systems, both under rapid developments nowadays. Standalone positioning solutions based on such systems complementary to GNSS can be beneficial in situations where GNSS signal is highly affected by interferences, such as jammers and spoofers, while hybrid GNSS and non-GNSS solutions making use of LEO and terrestrial IoT signals as signals of opportunity can improve the achievable positioning accuracy in a wide variety of scenarios. Comparative research of performance bounds achievable through MEO, LEO, and terrestrial IoT signals are still hard to find in the current literature. It is the goal of this paper to introduce a unified framework to compare these three system types, based on geometry matrices and error modeling, and to present a performance analysis in terms of Geometric Dilution of Precision (GDOP) and positioning accuracy bounds.

Index Terms—Medium Earth Orbit (MEO), Global Navigation Satellite Systems (GNSS), Low Earth Orbit (LEO) satellites, Internet of Things (IoT) terrestrial network, Positioning, Geometric Dilution of Precision (GDOP)

I. INTRODUCTION, STATE-OF-THE-ART-REVIEW, AND PAPER CONTRIBUTIONS

THERE are currently four Global Navigation Satellite Systems (GNSS), operating mostly in Medium Earth Orbits (MEO), namely the European Galileo, the US Navstar GPS, the Russian GLONASS, and the Chinese Beidou systems. Beidou system has also some of the satellites placed in the Geo-stationary Orbits (GEO), but since they are not contributing to the global/worldwide coverage targets, GEO satellites are not part of this work. GNSS solutions are able to achieve meter (m) and even sub-m positioning accuracy with multi-frequency multi-system receivers as long as they operate in outdoor and clear sky scenarios. In densely urban and indoor scenarios, the GNSS-based positioning and navigation is not always reliable [1], due to multipath and and Non Line of Sight (NLOS) propagation, and low Carrier-to-Noise-ratios (CNR). In addition, more and more interferences in GNSS bands, such as jamming and spoofing [2] have been recorded in the GNSS

bands. Therefore, complementary navigation and positioning solutions are increasingly needed, in order to cope better with intentional and unintentional interferences and to satisfy the demand for accurate indoor and urban navigation.

In addition to existing MEO satellites on sky, a wide range of Low Earth Orbit (LEO) satellite networks are currently emerging or under developments, such as SpaceX Starlink, Amazon Kuiper, OneWeb, BlackSky Global, Myriota, IceEye, etc. [3], [4], [5], [6]. LEO satellite systems are distributed at altitudes from a few hundred km (from the Earth surface) to a few thousand km. LEO constellations are characterized by having a lower transmission delay and typically a lower transmitting power with respect to MEO and GEO constellations, due to the LEO orbit proximity to the Earth. However, LEO constellations suffer from higher Doppler shifts due to their increased speeds compared to MEO satellites [7]. This Doppler effects can, in theory, enable an accurate Doppler-based positioning, but our recent studies in [6] showed that the theoretical bounds of Doppler-based positioning accuracy with LEO satellites is still much worse than the theoretical bounds of code-based positioning accuracy. Also, more LEO satellites are needed to offer coverage of the whole Earth than MEO satellites, due to the fact that LEO satellites are closer to the Earth surface than MEO ones, and therefore they cover less area. In addition, LEO satellites are visible for a lower time in a specific location (since satellite orbital speeds are higher in LEO than in MEO). Moreover, LEO satellites typically can offer a lower lifetime (mainly due to the phenomena called orbital decay, in which the satellites need to be constantly re-boosted because of the earth attraction force).

Finally, a third possible solutions for worldwide coverage to complement the satellite-based positioning may be based on the emerging terrestrial low-power long-range Internet of Things (IoT) networks, such as LoRa, Sigfox, or NarrowBand-IoT (NB-IoT) [8], [9]. Terrestrial IoT networks offers' the lowest delays and, arguably, also the lowest 'launching' (i.e., deployment) costs, but they need significantly more access points or transmitters to achieve similar coverage levels as MEO and LEO networks. In addition, achieving a good coverage in out-of-land areas (e.g., deep forests, oceans, seas, etc.) is much more challenging than with satellite-based systems.

While MEO satellites have been traditionally used for navigation purposes and current multi-system multi-frequency GNSS receivers can reach sub-meter accuracies and very good coverage outdoors [10], the use of LEO and IoT networks for positioning and navigation purposes is still in research phase.

R. Morales Ferre and E.S. Lohan are with the Electrical Engineering Unit, Tampere University, Finland, e-mails: {ruben.moralesferre,elena-simona.lohan}@tuni.fi.

For example, Doppler-based positioning with LEO satellites has been investigated in [11], [6], [12].

In general, Dilution of Precision (DOP) metric has been extensively studied in the context of satellite communications and navigation, as a metric conveying useful information about the attainable coverage and achievable performances with a certain metric, Generally speaking, one can look at five DOP types, namely: Horizontal DOP (HDOP), Vertical DOP (VDOP), Position (3D) DOP (PDOP), Time DOP (TDOP), and Geometric DOP (GDOP).

The main focus in our work will be on GDOP, defined later in Section II-B. The reason of focusing on GDOP is because GDOP is a metric that can be related to both the coverage and the positioning accuracy that a certain system can offer and it illustrates how well geometrically distributed are the transmitters (e.g., relative geometrical distribution of satellites on the sky or terrestrial access points or base stations with respect to a certain user). Lower GDOP values will be related to better global/Earth coverage and better accuracy of the positioning solution [13], [14].

Studies comprising comparisons between LEO, MEO, and terrestrial positioning approaches are not easy to find in the current literature. Partial comparisons such as LEO with MEO can be found for example in [15], [16], [17], [18]. In [15] the authors performed a comparison between LEO, MEO, and GEO constellations, although no specific constellations were mentioned and studies were done under generic assumptions. The considered multiple access scheme in [15] was is Frequency Multiple Access (FDMA), which does not match with the Code Division Multiple Access (CDMA) used by most of the MEO GNSS systems nowadays. Thus, the results reported in [15], especially the ones concerning the interferences, cannot be directly compared or extrapolated to this work. In [16], [18] the authors compared MEO, GEO, and High Earth Orbit (HEO) constellations. In [16], the authors computed GDOP values as a function of different satellite orbit heights. Among other results, the authors in [16] showed that, the higher the altitude of the satellites is, the worse the GDOP is. In [18] the authors used PDOP measurements for comparing the different constellations. In [17] the authors compare specific LEO and MEO constellations in therms of number of satellites, position error and GDOP (Geometric Dilution of Precision), PDOP (Position Dilution of Precision), HDOP (Horizontal Dilution of Precision) and VDOP (Vertical Dilution of Precision) concluding that LEO constellations for navigation has the potential to add tremendous benefit in terms of Position Navigation and Timing (PNT) solution accuracy and resilience.

To sum up, while communication aspects in LEO, MEO, and even GEO satellites have been investigated so far for more than two decades, e.g. starting with [15], the possible benefits of LEO satellites and IoT terrestrial networks for positioning, as complementary methods to MEO GNSS satellites are still in incipient phase of study. For example, our previous work in [6] focused on a Geometric Dilution of Precision (GDOP) comparison between eight LEO constellations. Both code-based and Doppler-based GDOP were previously investigated by us in [6]. The focus in [6] was entirely on LEO constellations,

and no MEO or terrestrial networks were included in the comparison. Our results in [6] showed that the Doppler-based GDOP values are much higher than the code-based GDOP values, pointing out towards the fact that a position estimate obtained through a pure Doppler-based positioning method cannot be as accurate as the one obtained through code-ranging measurements. For this reason, this paper focuses only on code-based GDOP modeling. While the work in [6] only looked at the error-free GDOP, this paper extends the code-based GDOP modeling to also take into account the various channel impairments such as ionospheric, troposheric, and multipath delays, as well as receiver code-tracking loop effects, which are based on the available receiver bandwidth and signal modulations.

The main novel contributions in this paper are:

- Deriving the error-based code GDOP and corresponding positioning errors in the presence of channel impairments and comparing it with the error-free code GDOP;
- Providing, for the first time in the literature to the best of the Authors' knowledge, a comprehensive comparison between MEO, LEO, and terrestrial IoT systems in terms of their suitability for positioning, by looking at the error-based code-GDOP and 3D positioning accuracy metrics, such as tracking error bounds and estimated average variance of the positioning errors;
- Offering a unified framework to compare current and emerging systems, based on geometry matrices with un-synchronized systems, modulation-dependent Power Spectral Densities (PSD), and models of various channel errors, such as ionospheric and tropospheric error models for satellite signals, Carrier-to-Noise Ratio (C/N_0), and multipath error models for various signal types;
- Showing the potential of LEO and IoT systems as future signals of opportunity (SoO) to complement MEO-based positioning;
- Giving specific examples of achievable GDOP and positioning accuracies in a selected geographical area, under the assumption of channel and receiver errors for eight selected LEO, MEO, and IoT systems.

II. UNIFIED THEORETICAL MODELING

In any positioning system, one of the factors influencing the achievable positioning error is the relative geometry between the transmitters (e.g., base stations or access points for terrestrial-based navigation and satellites for satellite-based navigation) and the mobile receiver [13]. This geometry-related metric, as also mentioned in Section I, is called dilution of precision (DOP). Besides the geometry of the transmitters (measured via GDOP), the main sources of error are due to: atmospheric effects for satellite signals (basically the troposphere and ionosphere), due to multipath effects (for both satellite and terrestrial signals), and due to other noises over the channel and receiver tracking loops when the positioning estimation relies on code and timing measurements [19]. The model adopted in what follows assumes time-based measurements for all considered systems. Time-based measurements have the potential of higher accuracy than the

received-signal-strength measurements and they do not require antenna arrays as required by the angle-of-arrival and angle-of-departure measurements. Also, for a fairer comparison, independent on details on receiver-tracking loops, we assume that the tracking error variances due to noise are given by the well-known Cramer Rao Lower Bound (CRLB), which is dependent only on the system bandwidth and on the system modulation type which shapes the PSD.

A. Geometry matrix

In a generic case with K unsynchronized systems to be used in a hybrid manner for obtaining a positioning solution, each having $N_k, k = 1, \ldots, K$ transmitters, the geometry matrix $\mathbf{H}$, contains the unit vectors pointing from the Taylor linearization point (i.e., prior estimate of the mobile position) to the location of the i_k-th transmitter, $i_k = 1, \ldots, N_k$ of the k-th positioning system, $k = 1, \ldots, K$ when solving a least squares (LS) system of equations [13], [20], [21]. $\mathbf{H}$ is given by [13], [6]:

$$\mathbf{H} \triangleq \begin{bmatrix} h_{x,1,1} & h_{y,1,1} & h_{z,1,1} & 1 & 0 \cdots 0 \\ h_{x,1,2} & h_{y,1,2} & h_{z,1,2} & 1 & 0 \cdots 0 \\ \vdots & \vdots & \vdots & & \vdots \\ h_{x,1,N_1} & h_{y,1,N_1} & h_{z,1,N_1} & 1 & 0 \cdots 0 \\ h_{x,2,1} & h_{y,2,1} & h_{z,2,1} & 0 & 1 \cdots 0 \\ \vdots & \vdots & \vdots & & \vdots \\ h_{x,2,N_2} & h_{y,2,N_2} & h_{z,2,N_2} & 0 & 1 \cdots 0 \\ \vdots & \vdots & \vdots & & \vdots \\ h_{x,K,N_K} & h_{y,K,N_K} & h_{z,K,N_K} & 0 & 0 \cdots 1 \end{bmatrix}, \quad (1)$$

where $h_{x,k,i} = \dfrac{x_{Tx_{k,i_k}} - x}{R_{k,i_k}}$, $h_{y,k,i_k} = \dfrac{y_{Tx_{k,i_k}} - y}{R_{k,i_k}}$ and $h_{z,k,i_k} = \dfrac{z_{Tx_{k,i_k}} - z}{R_{k,i_k}}$ are the components of the unit vector from the receiver to the i_k-th transmitter of the k-th positioning system under consideration ($i_k = 1, \ldots, N_k$) in the k-th positioning system ($k = 1, \ldots, K$). In this model, it is assumed that the different transmitters within one system k are synchronized, but the different systems are not synchronized between them - that is why the last columns from fourth to the last column $K + 3$ contains sequences of 1s (for synchronized transmitters) and 0s (for unsynchronized transmitters). Clearly, the model in eq. (1) can be expanded straightforwardly also to unsynchronized transmitters within the same system, but for clarity purposes and for a fairer comparison with the synchronized MEO systems, we will adopt the assumption of synchronized transmitters per system. Above, $x_{Tx_{k,i_k}}, y_{Tx_{k,i_k}}, z_{Tx_{k,i_k}}$ are the i_kth transmitter coordinates, x, y, z are the mobile user coordinates and R_{k,i_k} is the pseudorange between the user coordinates and the i_k-th satellite in the k-th positioning system, defined as

$$R_{k,i_k} = \sqrt{(x_{Tx_{k,i_k}} - x)^2 + (y_{Tx_{k,i_k}} - y)^2 + (z_{Tx_{k,i_k}} - z)^2} \quad (2)$$

As above-mentioned, the last K columns in Eq. (1) stand for the clock error factors, in order to take into account the different clock errors of different, unsynchronized, systems. As a side note, the simplified equation for H under the assumption of all considered transmitters/systems to be synchronized can be found in [6].

B. Code-GDOP metric in the absence of errors

For calculating the error-free code GDOP, one needs to compute first the measurement matrix $\mathbf{H}$, as shown in Eq. (1). After $\mathbf{H}$ is obtained, we can compute the error-free matrix $\mathbf{Q}_{ef}$ as

$$\mathbf{Q}_{ef} \triangleq (\mathbf{H^T H})^{-1} \in \mathcal{R}^{(\mathbf{K+3}) \times (\mathbf{K+3})} \quad (3)$$

with $\mathbf{Q}_{ef}$ being a $(K + 3) \times (K + 3)$ real-valued matrix.

Finally, the error-free code GDOP γ_{ef} is defined as the square-root of the trace of the error-free matrix $\mathbf{Q}_{ef}$, i.e. $\gamma_{ef} = \sqrt{sum(diag(\mathbf{Q}_{ef}))}$.

The values of the code-GDOP can be classified as: [13], [6]: code GDOP values below 2 are excellent, those between 2 and 10 are good-to-moderate, and those above 10 are fair-to-poor values. The positioning performance decreases when the code-GDOP value increases.

At its turns, the error-free positioning error variance in x, y, and x directions can be computed from Eq. (3) as the first three diagonal components of $\mathbf{Q}_{ef}$ matrix, namely $\mathbf{Q}_{ef}(i, i), i = 1, 2, 3$. The average variance of the positioning error σ_{pos}^2 in x,y,z directions will be thus $\sigma_{pos}^2 = \dfrac{\mathbf{Q}_{ef}(1, 1) + \mathbf{Q}_{ef}(2, 2) + \mathbf{Q}_{ef}(3, 3)}{3}$.

C. Sources of errors and error models

In this section we discuss five main error sources and we describe the error models used during our simulations. They are based on the existing literature [19], [22] and references therein.

1) Ionospheric error model: The satellite signals coming from MEO and LEO satellites are affected by the random movement of electrons in the ionospheric layer. The ionosphere is the layer of atmosphere comprised between about 80 km and 600 km above the Earth surface. The signals coming from satellites are randomly delayed when passing through ionospheric layer, due to the presence of electrically charged particles. Such delays can cause significant positioning errors if they are not compensated at the receiver. Ionospheric errors are, in general, the highest errors among the other error sources in satellite-positioning systems [13]. Terrestrial transmissions are not affected by the ionosphere. The ionospheric errors can usually be removed in dual-frequency receivers, based on the fact that same ionospheric layer is crossed by both frequencies and there is a non-linear dependence between the delays and the frequencies, depending on the same proportionality factor, namely the ionosphere electron content [13]. In single frequency receivers, ionospheric errors can also be corrected, to a certain extent, by using an ionospheric model, such as Klobuchar [23] or NeQuick [24].

In what follows, we adopt an exponential-variance ionosphere model, similar with [24], [19], [25],

$$\sigma_{Iono_{k,i_k}}^2 = \left(1 + \delta \exp\left(-\frac{el_{k,i_k}}{el_{ref}}\right)\right)^2 \quad (4)$$

where $\sigma^2_{Iono_{k,i_k}}$ is the delay error variance due to the random ionospheric delays for the i_k-th satellite of the k-th system under consideration, δ is a constant related to the maximum expected ionospheric error (e.g., $\delta = 10$ in our simulations, as in [19],[24], where the maximum ionospheric error after Klobuchar correction was below 10 m); el_{k,i_k} is the satellite elevation angle for the i_k-th satellite of the k-th system and and el_{ref} is a reference elevation angle or elevation mask, below which we assume the received signals become too weak and are not used on the positioning solution (taken equal to $10 \deg$ in our simulations). It is to be noticed that there are other ionospheric delay models in the literature such as sin-shaped [25]. One of the advantages of the model in eq. (4) is that it was found to be more accurate than other existing models in the literature [25] and that, by adequately fitting δ and el_{ref} parameters based on measurements and least-squares fitting, one can adapt it to a variety of situations, including MEO and LEO systems. For a fair comparison between LEO and MEO systems, the same model, as given in Eq. (4) was adopted for both. For the terrestrial IoT systems, $\sigma^2_{Iono_{k,i_k}} = 0$, as there is no ionospheric layer in the wireless path of the IoT signal.

2) Tropospheric error model: [23], [26] The troposphere is the layer of atmosphere closest to the Earth's surface, comprised from the earth surface to 8/15 km. The variations in tropospheric delay are basically caused by the changing humidity, temperature and atmospheric pressure. The tropospheric error is usually on the range of a few centimeters [27], [24], [23]. Examples of tropospheric error variance models can be found in [23], [28]. During our simulations we did not specifically model the tropospheric error, but we rather combined it jointly with the clock and orbit errors (see also Sec. II-C6) and assumed them to be constant within the simulations.

3) Multipath error model: Multipath errors are those that occur due to the presence of Non-Line-of-Sight (NLOS) components in addition to Line-of-Sight (LOS) components. In some cases, LOS can be even absent (e.g., due to obstructions such as tall buildings that may occur in the signal's path). Multipath signals (i.e., NLOS or LOS+NLOS cases) differ from the LOS signal in power, code delay, carrier phase, and frequency [19], [29], [30], [31]. In our simulations using MEO and LEO satellite-based positioning we have used the aeronautical multipath error model [27], [24], [13], which defines the error variance $\sigma^2_{mp_{k,i_k}}$ due to multipath as:

$$\sigma^2_{mp_{k,i_k}} = 0.13 + 0.53 \exp\left(-\frac{el_{k,i_k}}{el_{ref}}\right) \qquad (5)$$

where el_{k,i_k} is the i_k-th satellite of the k-th system satellite elevation angle and el_{ref} is a reference elevation angle. For terrestrial-based systems, only narrowband IoT systems such as LoRa were considered. Narrowband systems are known for their high robustness to multipath, due to the fact that their bandwidth is much below the channel coherence bandwidth, especially in mixed indoor-outdoor communications, thus $\sigma^2_{mp_{k,i_k}}$ is close to zero. For a fair comparison, we made the assumption that Eq. (5) still holds for $el_{k,i_k} = 0$, exhibiting thus a multipath error variance of maximum 0.66m for the terrestrial IoT system.

4) Carrier-to-Noise Ratio model: The tracking error variance based on timing estimates for any receivers is proportional to the Carrier-to-Noise Ratio (C/N_0) at the receiver. Clearly, for satellite transmitters, the satellites with higher elevation have a higher C/N_0 than those with a lower elevation. The adopted model for estimating the C/N_0 is based on the premise than a lower elevation will provide a lower C/N_0 and it is defined as follows:

$$C/N_0(el_{k,i_k}) = C/N_{0,ref} + 20log(el_{k,i_k}) \qquad (6)$$

where el_{k,i_k} is the i_k-th satellite of the k-th system satellite elevation angle and $C/N_{0,ref}$ is the reference C/N_0 at $90 \deg$ elevation, which is set equal to 45 dB-Hz. In our examples, we considered a nominal C/N_0 of 45 dBHz in order to have a fair comparison between different systems and because 45 dBHz is at the lower limit of the typical nominal interval for GNSS outdoors. Nevertheless, the presented models are generic and can apply to any C/N_0.

For terrestrial transmitters, C/N_0 can be computed based on link budgets, by taking into account the transmitter-receiver distances. For a fair comparison, in our model, we assumed an average C/N_0 for terrestrial transmitters equal to the reference $(C/N_0)_{ref}$ from the satellite transmitters.

5) Tracking-noise variance error model: This error is due to the receiver estimation errors during the timing/code-based estimation [32], [33], [34]. For example, the code delay estimation is typically done in spread spectrum receivers such as GNSS receivers, by what is known as a Delay Tracking Loop (DLL), by measuring the differences between an early and late correlation (spaced less than one chip apart) [34], [35], [36], [37]. For a generic approach, independent on the receiver delay tracking loops, one can adopt the CRLB estimates [22]. CRLB variance bounds are valid for any signal type, namely for both satellite and terrestrial-based positioning and they depend only on the receiver bandwidth and the received signal power spectral density $G(f)$, or more specifically, on the root-mean-square (RMS) bandwidth at the receiver: [22]:

$$\sigma^2_{CRLB_{k,i_k}} = \frac{\int_{-B_W/2}^{B_W/2} G(f)df}{2(2\pi^2)C/N_0 \int_{-B_W/2}^{B_W/2} f^2 G(f)df} \qquad (7)$$

where $\sigma^2_{CRLBTrack_{k,i_k}}$ is the tracking variance error in squared seconds for the signal received from the i_k-th transmitter of the k-th system under consideration and B_W is the receiver signal bandwidth. Above, the factor $\int_{-B_W/2}^{B_W/2} f^2 G(f)df$ represents the RMS bandwidth and the formula above shows that the CRLB bound in variance is inversely proportional to the normalized RMS bandwidth at the receiver. The power spectral density $G(f)$ at its turns, depends on the signal modulation. Detailed expressions for $G(f)$ for GNSS signals can be found for example in [22], [19]. Generally speaking, for a BPSK-modulated signal, as often encountered in LEO satellites, if we assume independently and identically distributed transmitted symbols and ideal pulse shaping, the $G(f)$ can be approximated by [22]

$$G(f) = \left(\frac{sin(\pi f/B_W)}{\pi f}\right)^2 \qquad (8)$$

For Chirp Spread Spectrum (CSS) modulations as those used in LoRa terrestrial IoT systems, the exact PSD expressions can be found for example in [38], where it was also shown that a good approximation for narrowband CSS systems such as LoRa is a constant PSD $G(f) = 0.97$. This is also the approximation we adopted in our simulations.

Similarly, for Gaussian Minimum Shift Keying Modulations (GMSK), as those used for example in LEO Myriota signals, the exact PSD expressions can be found in [39]. Again, for narrowband communications as those employed in Myriota, the GMSK PSD can be approximated via $G(f) = 0.96$. [39]

More details on the compared MEO, LEO, and IoT systems are given in Table I. As an example, the tracking error standard deviation expressed in meters, i.e. $c\sigma_{CRLBTrack_{k,i_k}}$, is shown in Fig. 1 (here c is the speed of light).
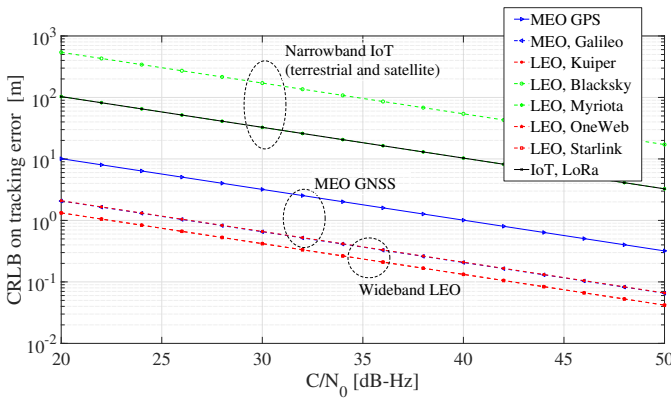

Fig. 1: Examples of CRLB tracking error bounds [m], based on the parameters in Table I .

Clearly, narrowband systems such as LoRa, Myriota, and BlackSky Global, have high tracking error standard deviations, of the order of several hundred of meters. The MEO GNSS satellites (e.g., Galileo E1 and GPS L1 considered in Fig. 1) have moderate tracking error standard deviations, of the order of few meters, and the wideband LEO systems employing hundreds of MHz of bandwidth can reach centimeter levels in the tracking error standard deviation, thanks to their higher bandwidths.

6) Clock, Orbit, and other Error Variances: The atomic clocks used in satellite positioning are extremely precise, although they cannot avoid a small drift. similarly, satellites travel in very precise, well known orbits, But the orbits do vary as well a small amount. The satellite clock and orbit errors are typically below 1.5 m [27]. In our simulations the clock and orbit error variances are put together with in an additive white Gaussian noise component of zero mean and a constant $\sigma^2_{N_{k,i_k}}$ variance that includes also the tropospheric error, which is defined as

$$\sigma^2_{N_{k,i_k}} = \sigma^2_{Clock_{k,i_k}} + \sigma^2_{Orbit_{k,i_k}} + \sigma^2_{Tropo_{k,i_k}} \quad (9)$$

where σ^2_{Noise,k,i_k} includes the clock error variance $\sigma^2_{Clock_{k,i_k}}$, orbit error variance $\sigma^2_{Orbit_{k,i_k}}$ and tropospheric error variance $\sigma^2_{Tropo_{k,i_k}}$. For modelling it during the satellite based positioning simulations, we assumed a constant $\sigma^2_{Noise_{k,i_k}}$ error

for all satellite transmitters, set at a maximum bound of 2 m This value was set based on the literature models on the sum of the tropospheric, clock, and orbital errors, which are typically below this range [19]. For terrestrial transmitters, there are no orbital and tropospheric errors (i.e., $\sigma^2_{Orbit_{k,i_k}} = 0$ and $\sigma^2_{Tropo_{k,i_k}} = 0$), but we still assumed a constant 2-m error for the clock error for a fair comparison with satellite transmitters, as in terrestrial IoT case, due to typically lower-cost transmitters and receivers, the clock errors are expected to be higher than in the satellite-transmitter case.

D. GDOP unified model with sources of error

To include the sources of error in the calculation of the DOP measurements, we first need to define the diagonal error covariance matrix for the k-th system under consideration, $k = 1, \dots, K$ as

$$\boldsymbol{\Sigma_k} \triangleq \begin{bmatrix} \sigma^2_{Tot_{k,1}} & 0 & \dots & 0 \\ 0 & \ddots & & \vdots \\ \vdots & & \ddots & 0 \\ 0 & \dots & 0 & \sigma^2_{Tot_{k,N_k}} \end{bmatrix} \quad (10)$$

where $\sigma^2_{Tot_{k,i_k}}$ is the total variance error that contains the variance errors from Sec. II-C for the i_k-th satellite in the k-th positioning system, namely:

$$\sigma^2_{Tot_{k,i_k}} = \sigma^2_{Iono_{k,i_k}} + \sigma^2_{N_{k,i_k}} + \sigma^2_{mp_{k,i_k}} + \sigma^2_{CRLB_{k,i_k}} \quad (11)$$

Then we can compute the $\mathbf{Q} \in \mathcal{R}^{(K+3) \times (K+3)}$ matrix for K multi-positioning systems in the presence of errors as:

$$\mathbf{Q} = (\mathbf{H}^T (\Sigma_{all})^{-1} \mathbf{H})^{-1} \quad (12)$$

where $\Sigma_{all} = diag(\Sigma_1, \dots, \Sigma_K)$ is a $\left(\sum_{k=1}^{K} N_k\right) \times \left(\sum_{k=1}^{K} N_k\right)$ diagonal error covariance matrix containing the error variances from all K considered systems and from all N_k visible transmitters per system. Finally, the GDOP γ and the receiver position error variance σ^2_{pos} can be derived from the diagonal elements of $\mathbf{Q}$ as shown in section II-B. We get:

$$\text{GDOP}: \gamma = \sqrt{\sum_{i=1}^{K+3} \mathbf{Q}(i,i)} \quad (13)$$

$$\text{Pos error}: \sigma^2_{pos} = \frac{\sum_{i=1}^{3} \mathbf{Q}(i,i)}{3}$$

It is to be noticed that the summation index in the lower term in Eq. (13) contains only the first three diagonal terms of matrix $\mathbf{Q}$. It is straightforward to see that the standard deviation of the positioning error σ_{pos} is thus upper bounded by the error-based GDOP divided by $\sqrt{3}$, i.e.: $\sigma_{pos} \leq \gamma/\sqrt{3}$. It follows that the error-based GDOP can give a clear intuition regarding the achievable positioning accuracies with various systems. Concrete examples will be provided in Section III.

The diagonal error matrix assumption from Eq. (10) holds if one assumes that various errors coming from different transmitter-receiver paths are uncorrelated. This is not a un-realistic assumption, as transmitters are usually widely apart (especially in satellite systems under consideration), thus the

corresponding wireless channels (and associated errors) are uncorrelated.

III. SIMULATION-BASED RESULTS

A. Systems considered in our comparison

Table I summarizes the main parameters of interest of the eight considered systems in our further simulations, namely five LEO constellations, two MEO constellations, and one terrestrial IoT constellation. The given parameters include the number of transmitters (i.e., number of satellites for LEO and MEO systems and number of access points for terrestrial IoT system), the carrier frequencies in uses, the available receiver bandwidth, the modulation types to be employed in the considered systems (an N/A value means the information is not available yet), and the parameters we used in our simulations. The number of transmitters refers to the total number of transmitters planned for a certain LEO or MEO system, with the note that currently, for LEO systems, not all of these satellite transmitters have been already launched. For terrestrial IoT access points, this transmitter number is, of course, variable, and we have shown in brackets the number of transmitters assumed in our model, starting from the hypotheses of one IoT transmitter per km^2 and uniform distribution of IoT transmitters across the considered region. This is not an unreasonable assumption based on current figures of LoRa deployments in various EU countries, and it has been taken a bit on the optimistic side, in order to see the maximum achievable performances with LoRa IoT.

Fig. 2 shows an example of constellation orbits for one MEO (i.e., GPS) and one LEO (i.e. Myriota) system at a time, to illustrate their relative proximity to Earth and the fact that LEO constellations are much richer in the number of satellites and orbits than MEO systems, a fact also seen previously in Table I.
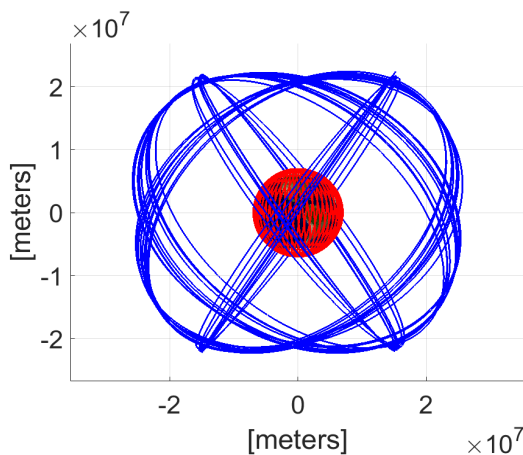

Fig. 2: Example of orbital planes of two constellations: Myriota (red) and GPS (blue).

B. GDOP-based results

For clarity and fairness-of-comparison purposes, the results were run for a certain geographical region (in this case,

European region and neighbourhoods) and considering only the terrestrial (out-of-sea) receiver location on Earth, as IoT access points are unlikely to offer good coverage outside land (e.g., on ships sailing the seas). Nevertheless, the results can be straightforwardly extended with the presented models to the full Earth coverage. 10000 Monte Carlo runs were used to generate 10000 random receiver locations in the considered geographical region (Europe and neighbourhoods), with latitudes between 30° and 74.99^o and longitudes between -25° and $+45^0$. For each of these 10000 runs, the satellites or terrestrial transmitters in view from different systems were calculated, and the models from Section II were used to compute the error-based GDOP values. The constellations were simulated via own developed Matlab-based simulator, relying on input assumptions on the orbital parameters of each LEO and MEO constellation, and on the number and distribution of IoT transmitters on Earth for IoT studies. The satellite positions were determined according to the Kepler equations of motion [40], [41]. In each Monte Carlo simulation, the user position was set randomly within the pre-defined geographical area (e.g. Europe and neighbourhoods) and the DOP was computed.

Fig. 3, Fig. 4, Fig. 5, and Fig. 6 show the error-based GDOP contour maps over Europe, for LEO, MEO, and IoT considered systems, respectively. The average error-based GDOP is also shown in the figures' captions for an easy comparison. For comparison purposes, the right-hand side of these plots also shows the error-free GDOP; i.e., a GDOP computed with eqs. (12,13) under the assumption of an identity Σ_{all} matrix.

While LEO constellations have a significantly higher number of satellites in the constellation than MEO constellations, which can be seen by a higher level of red-colored regions in Fig. 3 and Fig. 4 than in Fig. 5, they are not currently optimized for positioning purposes. This means that, the achievable error-based code GDOP for LEO is not significantly higher than for MEO systems (details are further given in Table II) even for LEO constellations with 100 times more satellites than MEO constellations. The average error-based code GDOP decrease for LEO satellites versus MEO satellites is 3.4 times. Interestingly enough, the best code-DOP-based results in the European region are not achieved with the largest constellation (Starlink), but with the second-largest constellation (Kuiper), pointing out to the fact that Kuiper signals might be more suitable as signals of opportunity for positioning than other LEO constellations (provided that this remains valid also in other Earth regions not considered here).

The number of points with error-based GDOP higher than 10 is shown in Table II. The mean and variance of error-based code GDOP are also shown and they are computed over the non-outlier points (i.e., over all points with good-to-moderate error-based code GDOP (i.e., below 10). Clearly, the satellite-based systems have much better coverage (less outliers) than the considered terrestrial IoT system, even when the network of IoT access points is very dense (one transmitter per km^2 as considered here). GPS has the best coverage over the European area (lowest amount of outliers) under the error-based GDOP considerations, followed by LEo Blacksky Global, LEO Myriota, and Galileo. In terms of the mean error-based GDOP over the covered points (i.e., non-outlier

TABLE I: Parameters of the considered constellations

Constellation	Name	Number of Tx	Carrier frequencies	BW	Modulation	Used parameters for CRLB computation
LEO	Amazon Kuiper	3236	Ka-band: 17.75-17.85 GHz 18.8-19.3 GHz 19.250-18.450 GHz 19.7-20.2 GHz	100 MHz	N/A	BW= 100 MHz BPSK modulation
	BlackSky Global	60	X-band: 8.025 - 8.4 GHz	30 KHz	N/A	BW= 30 kHz BPSK modulation
	Myriota	50	VHF: 156-165 MHz UHF: 399-403	150 kHz	GMSK	BW= 150 kHz GMSK modulation
	OneWeb	80	Ku-band: 10.7–12.7 GHz V-band:37-55 GHz)	250 MHz	BPSK (Uplink) QPSK (Downlink)	BW=250 MHz QPSK modulation
	Space X / Starlink	11927	Ku-band: 10.7-12.75 GHz Ka-band: 17.8-18.6 GHz 18.8-19.3 GHz 37.5-42.5 GHz V-band: 37.5-42.5 GHz	250 MHz	OQPSK QAM (up to 64 QAM)	BW=250 MHz 2-QAM (BPSK) modulation
MEO	Galileo	30	L-band: 1559-1591 MHz (Galileo E1) 1164-1214 MHz (Galileo E5) 1260-1300 MHz (Galileo E6)	4-50 MHz	CBOC(+), CBOC(-), BPSK, AltBOC	BW=24 MHz CBOC(-) modulation
	GPS	31	L-band: 1563-1587 MHz (GPS L1) 1215-1237 MHz (GPS L2) 1164-1189 MHz (GPS L5)	4-20 MHz	BPSK, TMBOC	BW= 4MHz BPSK modulation
IoT	LoRa	1e5	ULF: 863-870 MHz (Europe) 902-928 MHz (USA) 923 MHz (Asia) 920-923 MHz (Korea) 865-867 MHz (India)	125-250 kHz	CSS	BW=125 kHz CSS modulation

points), the best performance is attained by LEO Kuiper system, followed by the terrestrial IoT, LEO Starlink, and LEO Blacksky Global. It is to be reminded that mean GDOP values below 2 are excellent, and whose below 10 are good-to-moderate.

C. Positioning accuracy results

The positioning contour plots (based on Eq. (13) for one representative system per considered types (LEO, MEO, IoT) are shown in Fig. 7. They clearly match with the GDOP contour plots illustrated in the previous section.

The mean and standard deviation of the positioning error computed in Eq. (13) are shown in Fig. 8 for the eight systems under consideration. While terrestrial IoT solutions give comparative average errors with the other systems, their standard deviation of the positioning error is significantly higher, meaning that they are less robust than the other signals of opportunity. It is out belief that robustness could be increased by optimizing the distribution of the terrestrial IoT transmitters (now assumed uniformly distributed), but an optimization-based deployment of IoT transmitters or gateways is unlikely to be feasible for the sole purpose of

enhancing the positioning targets; joint communication and positioning aspects must be considered. Among the LEO systems, also as determined based on GDOP analysis in the previous section, the Amazon Kuiper constellation gives the best positioning results as signals of opportunity, followed by Starlink. Surprisingly enough, the number of satellites in the constellation is not directly proportional with the expected mean and variance of the positioning errors; for example, Kuiper constellations, which has a lower number of satellites than Starlink, shows better performance than Starlink, and the narrowband IoT systems such as Myriota and Blacksky outperform OneWeb system, which has a higher number of satellites in its constellation. This similar scale of the performance in terms of mean position error is due to two facts: 1) that the geometry of the constellation may be rather similar with both high and low number of satellites, as the satellite constellation has not been optimized for positioning; ii) the mean position error and standard deviation error are only computed over the Earth points where at least minimum 4 satellites are in view. It can be also seen from Fig. 8 that most LEO considered systems have very promising performance in terms of positioning accuracy and have potential of being good complementary systems to the existing GNSS systems. The

(a) Blacksky constellation

(b) Blacksky constellation Error-free

(c) Myriota constellation
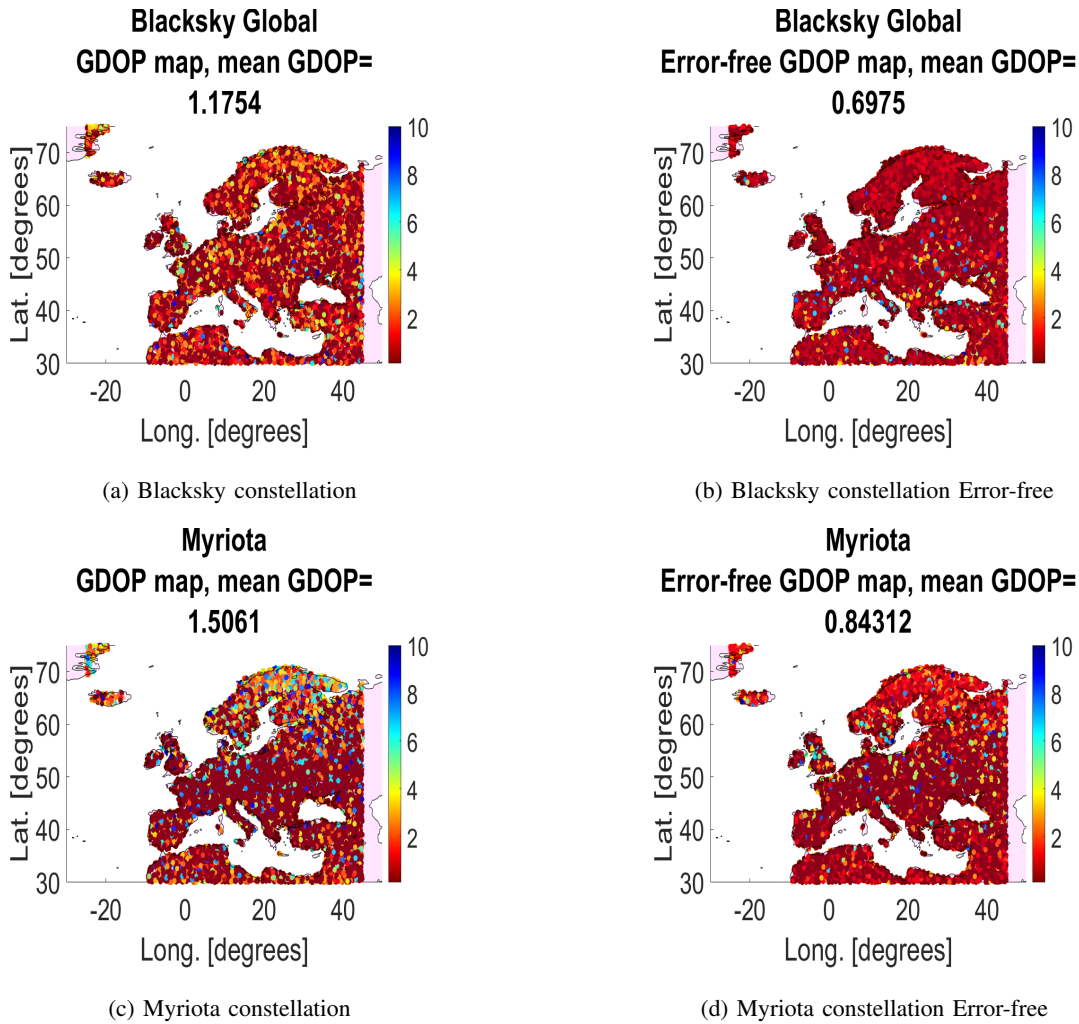
(d) Myriota constellation Error-free

Fig. 3: Comparison of error-based GDOP (left plots) and error-free GDOP (right plots) for two narrowband LEO satellite systems (Blacksky - upper plots and Myriota- lower plots).

terrestrial IoT systems are also promising in terms of average positioning errors, but their robustness needs to be improved in order to serve all areas with better performance. Fig. 9 shows the position error histogram for all the constellations analyzed in this work, after removing all outliers. It can be seen from Fig. 9 that the error distribution for terrestrial IoT and LEO systems is rather similar, in the sense that the most errors happen mostly between 0 and 2 meter. For MEO systems, the histogram is more spread than for LEO and IoT systems, which is also in agreement with the results presented in Table II.

IV. CONCLUSIONS AND OPEN ISSUES

In this paper we have derived an error-based code-GDOP metric and a positioning-error metric that enable a comparison between various satellite systems (LEO, MEO) and terrestrial IoT systems in terms of their performance as positioning systems. LEO and IoT systems are seen as potential signals for opportunity that may complement in the future the existing MEO GNSS constellations, either in a stand-alone mode (analyzed here) or in hybrid solutions (remaining as further

topic of research). We have applied the derived models for an example of a contained geographical area (here, Europe and surroundings), based on 10000 random Monte Carlo runs of uniformly distributed receiver locations in this area. We have showed that both LEO and IoT systems show promising results in terms of achievable GDOP and positioning accuracy as signals of opportunity.

In particular, LEO Kuiper constellation is the most promising among the considered signals-of-opportunity in terms of GDOP and achievable positioning errors. We believe that our error model paves the road towards more extensive analyses of LEO and terrestrial IoT systems as signals of opportunity for positioning, as new and more complex channel error models can be easily included in the current theoretical framework. In addition, once the signal modulations and bandwidths of the upcoming LEO systems are known, tighter bounds than CRLB on code tracking errors can be derived, by taking into account the specifics of each delay tracking unit as the LEO receivers.

Another open future research direction is the investigation of the beam-based and/or angle-based positioning of future LEO

(a) Kuiper GDOP measurements

(b) Kuiper Error-free GDOP measurements

(c) Oneweb GDOP measurements

(d) Oneweb Error-free GDOP measurements

(e) Starlink GDOP measurements
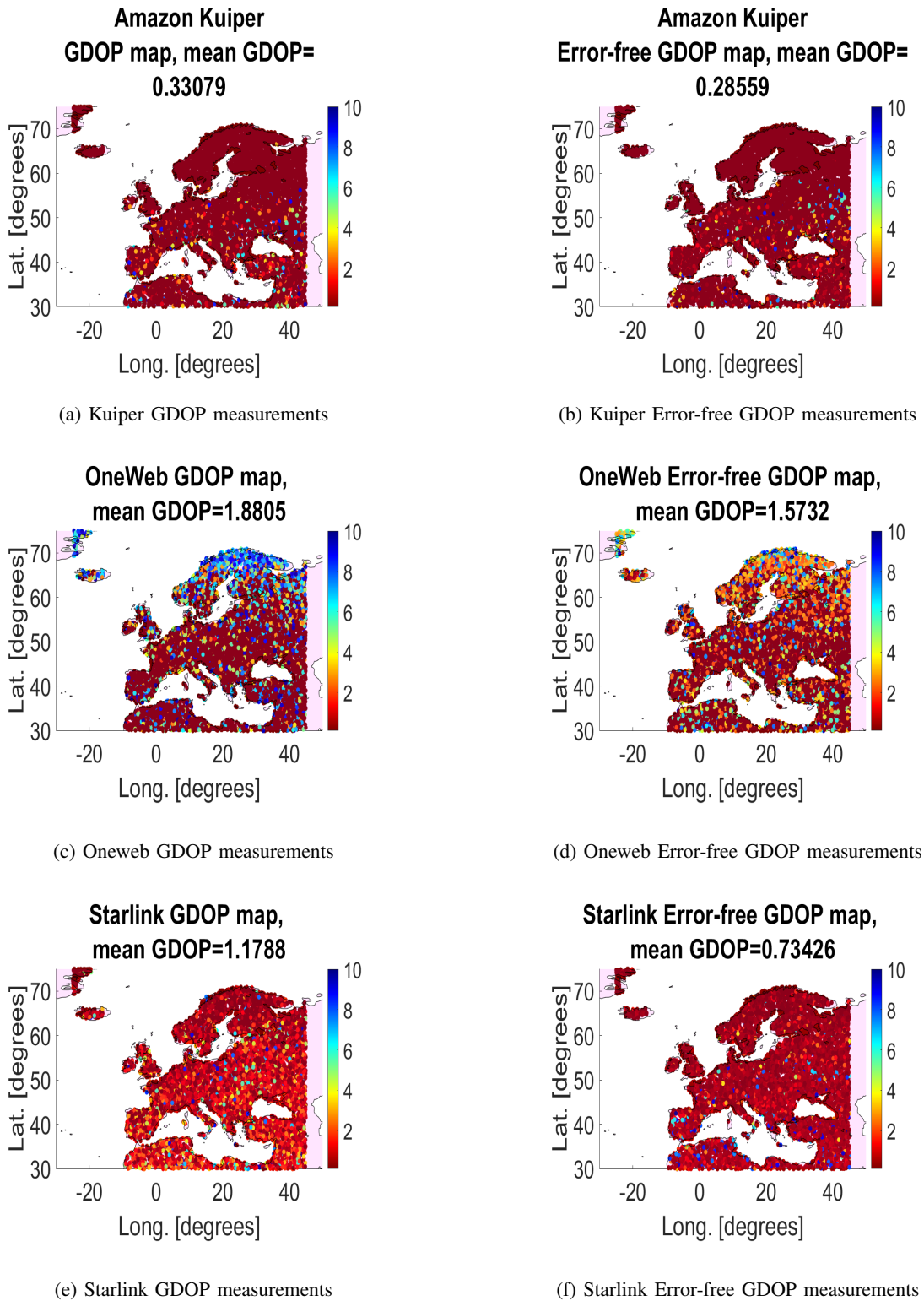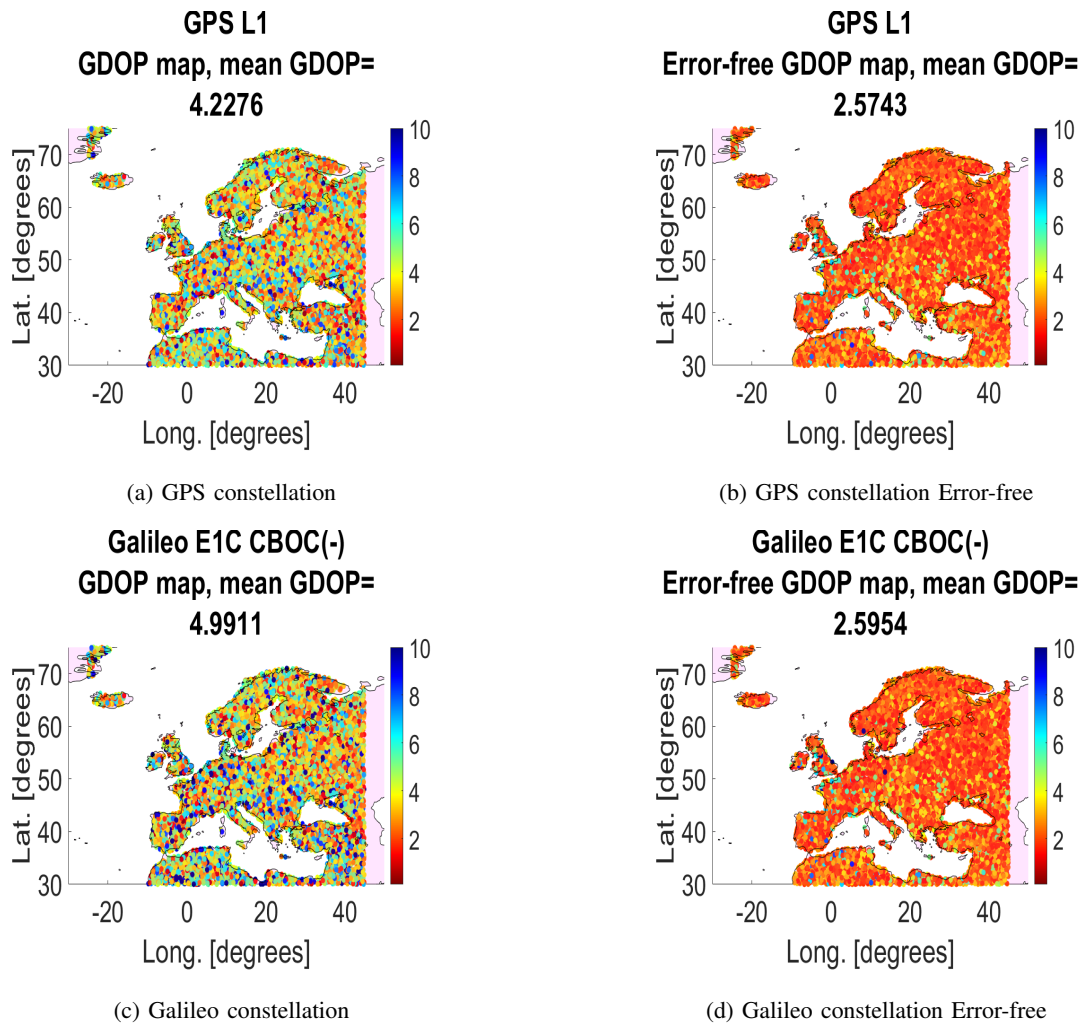
(f) Starlink Error-free GDOP measurements

Fig. 4: Comparison of error-based GDOP (left plots) and error-free GDOP (right plots) for three wideband LEO satellite systems (Kuiper - upper plots, OneWeb - middle plots, and Starlink - lower plots).

systems supporting high-order beamforming, in addition to the code-based positioning. Also, open for further research is the question of how one could design a new LEO constellation with a minimum amount satellites (i.e., minimum costs) that are needed to reach certain minimum coverage and positioning accuracy limits.

(a) GPS constellation

(b) GPS constellation Error-free

(c) Galileo constellation

(d) Galileo constellation Error-free

Fig. 5: Comparison of error-based GDOP (left plots) and error-free GDOP (right plots) for two MEO satellite systems (GPS L1 - upper plots and Galileo E1- lower plots).
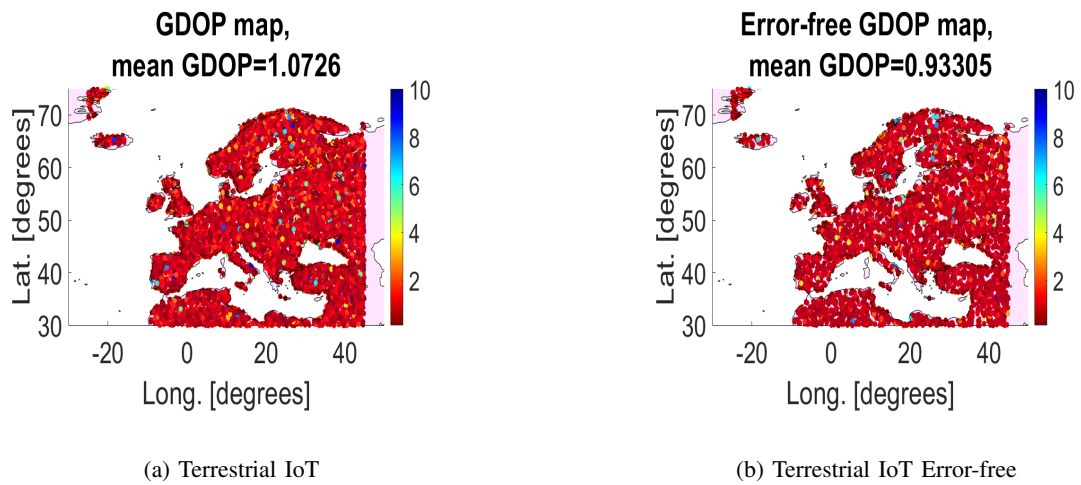

(a) Terrestrial IoT

(b) Terrestrial IoT Error-free

Fig. 6: Comparison of error-based GDOP (left plots) and error-free GDOP (right plots) for one terrestrial IoT system (LoRa).

TABLE II: Percentage of 'outliers', defined as terrestrial points with error-based GDOP higher than 10 i.e, fair-to-poor GDOP cases (European region and surroundings); mean and standard deviation of error-based code GDOP are also shown.

System	Outlier percentage	mean error-based GDOP [-]	standard deviation of error-based code GDOP [-]
LEO Blacksky Global	9.13 %	1.17	1.75
LEO Amazon Kuiper	23.87 %	0.33	1.31
LEO Myriota	11.66 %	1.50	2.45
LEO OneWeb	18.77 %	1.88	3.06
LEO SpaceX Starlink	23.47 %	1.17	1.57
MEO GPS	5.19 %	4.22	1.84
MEO Galileo	14.38 %	4.14	2.11
Terretrial LoRa IoT	65.2 %	1.07	1.05

REFERENCES

[1] X. Gan, B. Yu, X. Wang, Y. Yang, R. Jia, H. Zhang, C. Sheng, L. Huang, and B. Wang, "A new array pseudolites technology for high precision indoor positioning," *IEEE Access*, vol. 7, pp. 153 269–153 277, 2019.

[2] R. Morales-Ferre, P. Richter, E. Falletti, A. de la Fuente, and E. S. Lohan, "A survey on coping with intentional interference in satellite navigation for manned and unmanned aircraft," *IEEE Communications Surveys Tutorials*, vol. 22, no. 1, pp. 249–291, 2020.

[3] Y. Zhang, Z. Wang, Y. Huang, J. Ren, Y. Yin, Y. Liu, G. F. Pedersen, and M. Shen, "Deep neural network-based receiver for next-generation leo satellite communications," *IEEE Access*, vol. 8, pp. 222 109–222 116, 2020.

[4] S. Chen, S. Sun, and S. Kang, "System integration of terrestrial mobile communication and satellite communication —the trends, challenges and key technologies in b5g and 6g," *China Communications*, vol. 17, no. 12, pp. 156–171, 2020.

[5] A. Ivanov, R. Bychkov, and E. Tcatcorin, "Spatial resource management in leo satellite," *IEEE Transactions on Vehicular Technology*, pp. 1–1, 2020.

[6] R. Morales-Ferre, E. S. Lohan, G. Falco, and E. Falletti, "Gdop-based analysis of suitability of leo constellations for future satellite-based positioning," in *2020 IEEE International Conference on Wireless for Space and Extreme Environments (WiSEE)*, 2020, pp. 147–152.

[7] Y. Zhao, J. Cao, and Y. Li, "An improved timing synchronization method for eliminating large doppler shift in leo satellite system," in *2018 IEEE 18th International Conference on Communication Technology (ICCT)*, 2018, pp. 762–766.

[8] W. Ayoub, A. E. Samhat, F. Nouvel, M. Mroue, and J. Prévotet, "Internet of Mobile Things: Overview of LoRaWAN, DASH7, and NB-IoT in LPWANs Standards and Supported Mobility," *IEEE Communications Surveys Tutorials*, vol. 21, no. 2, pp. 1561–1581, 2019.

[9] W. Abdallah, S. Mnasri, N. Nasri, and T. Val, "Emergent iot wireless technologies beyond the year 2020: A comprehensive comparative analysis," in *2020 International Conference on Computing and Information Technology (ICCIT-1441)*, 2020, pp. 1–5.

[10] J. Bu, K. Yu, N. Qian, X. Zuo, and J. Chang, "Performance assessment of positioning based on multi-frequency multi-gnss observations: Signal quality, ppp and baseline solution," *IEEE Access*, vol. 9, pp. 5845–5861, 2021.

[11] W. Hsu and S. Jan, "Assessment of using doppler shift of leo satellites to aid gps positioning," in *2014 IEEE/ION Position, Location and Navigation Symposium - PLANS 2014*, 2014, pp. 1155–1161.

[12] A. Nardin, F. Dovis, and J. A. Fraire, "Empowering the tracking performance of leo pnt by means of meta-signals," in *2020 IEEE International Conference on Wireless for Space and Extreme Environments (WiSEE)*, 2020, pp. 153–158.

[13] E. D. Kaplan and C. J. Hegarty, Eds., *Understanding GPS: principles and applications*, 2nd ed. Artech House Publishers, 2006.

[14] V. Srilatha, I. Dutt, G. Sasi, B. Rao, S. Swapna, S. R. Babu, R. Goswami, and U. Kumari, "Investigation of GDOP for precise user position computation with all satellites in view and optimum four satellite configurations," *J. Ind. Geophys. Union*, vol. 13, 01 2009.

[15] F. Vatalaro, G. Corazza, C. Caini, and C. Ferrarelli, "Analysis of leo, meo, and geo global mobile satellite systems in the presence of interference and fading," *Selected Areas in Communications, IEEE Journal on*, vol. 13, pp. 291 – 300, 03 1995.

[16] V. Capuano, C. Botteron, and P.-A. Farine, "Gnss performances for meo, geo and heo," in *Space Communications and Navigation Symposium-Space-Based Navigation Systems and Services*, no. CONF, 2013.

[17] T. F. W. Tyler G. Reid, Andrew M. Neish and P. K. Enge, "Leveraging commercial broadband leo constellations for navigating," in *Proceedings of the 29th International Technical Meeting of the Satellite Division of The Institute of Navigation (ION GNSS+ 2016*, 2016, pp. 2300–2314.

[18] H. Liu, X. Cheng, T. Geshi, and J. Peng, "Gnss performance research for meo, geo, and heo," in *China Satellite Navigation Conference (CSNC) 2017 Proceedings: Volume III*, 05 2017, pp. 37–45.

[19] E. S. Lohan and K. Borre, "Accuracy limits in multi-gnss," *IEEE Transactions on Aerospace and Electronic Systems*, vol. 52, no. 5, pp. 2477–2494, 2016.

[20] P. Misra and P. Enge, *Global Positioning System: Signals, Measurements, and Performance*. Ganga-Jamuna Press, 2011. [Online]. Available: https://books.google.fi/books?id=5WJOywAACAAJ

[21] J. Nurmi, E. S. Lohan, S. Sand, H. Hurskainen *et al.*, *GALILEO positioning technology*. Springer, 2015, vol. 176.

[22] E. Simona Lohan, "Analytical performance of cboc-modulated galileo e1 signal using sine boc(1,1) receiver for mass-market applications," in *IEEE/ION Position, Location and Navigation Symposium*, 2010, pp. 245–253.

[23] R. Radovanovic, "Adjustment of satellite based ranging observations for precise positioning and deformation monitoring," 2002.

[24] P. Neri, L. Azoulai, and C. Macabiau, "Study of the temporal behavior of gps/galileo nse and raim for lpv200," in *Proceedings of the 24th International Technical Meeting of the Satellite Division of The Institute of Navigation (ION GNSS 2011)*, 2011, pp. 3796–3813.

[25] G. Kermarrec, "Stochastic modelling of gnss phase observations with focus on correlations," PhD dissertation, Karlsruhe Institute of Technology, 2017.

[26] R. S. RADOVANOVIC, N. EL-SHEIMY, and W. F. TESKEY, "Variance-covariance modeling of atmospheric errors for satellite-based network positioning," *NAVIGATION*, vol. 51, no. 2, pp. 161–170, 2004. [Online]. Available: https://onlinelibrary.wiley.com/doi/abs/10.1002/j.2161-4296.2004.tb00348.x

[27] A. Martineau, C. Macabiau, and M. Mabilleau, "Gnss raim assumptions for vertically guided approaches," in *Proceedings of ION GNSS*, 2009.

[28] N. E.-S. R. S. Radovanovic and W. F. Teskey, "Variance-covariance modelling of tropospheric errors for precise kinematic positioning via rigorous network adjustment," in *Proceedings of the International Symposium on Kinematic Systems in Geodesy Geomatics and Navigation*, 2001.

[29] M. Z. H. Bhuiyan and E. S. Lohan, "Multipath mitigation techniques for satellite-based positioning applications," in *Global Navigation Satellite Systems*, S. Jin, Ed. Rijeka: IntechOpen, 2012, ch. 17. [Online]. Available: https://doi.org/10.5772/29137

[30] M. Z. H. Bhuiyan, E. S. Lohan, and M. Renfors, "Code tracking algorithms for mitigating multipath effects in fading channels for satellite-
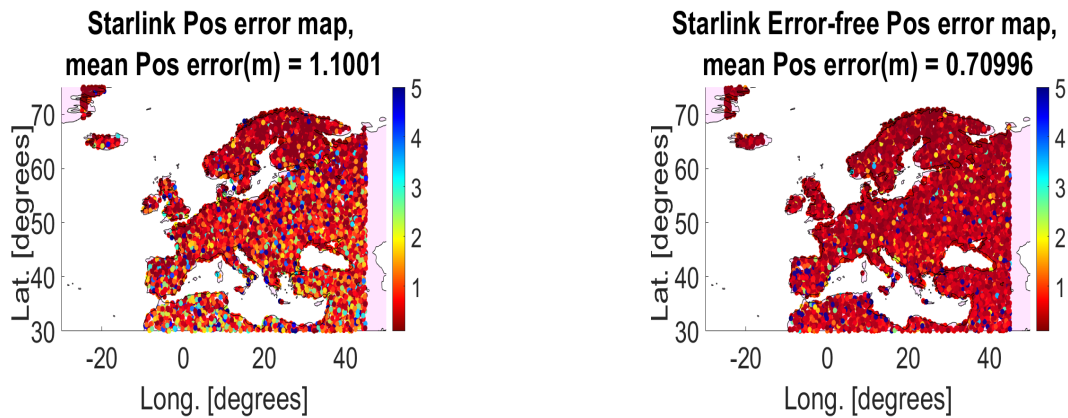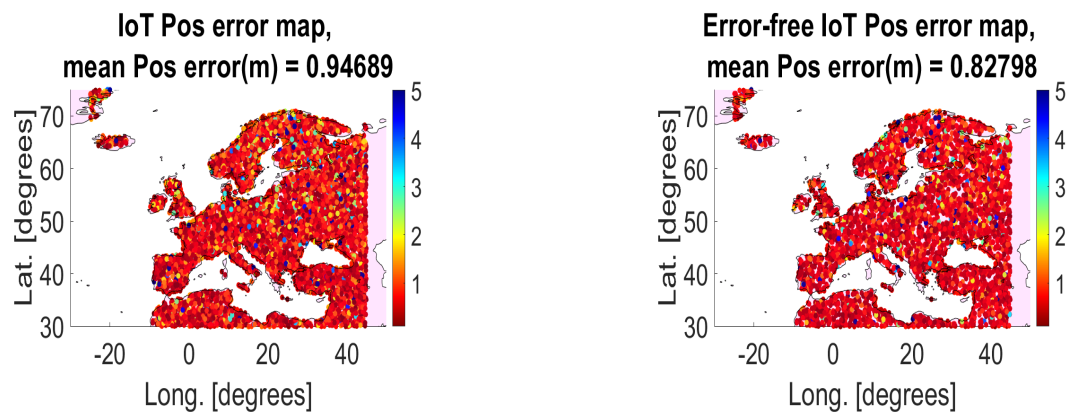
(a) Error-based positioning accuracy, Starlink constellation.

(b) Error-free positioning accuracy, Starlink constellation
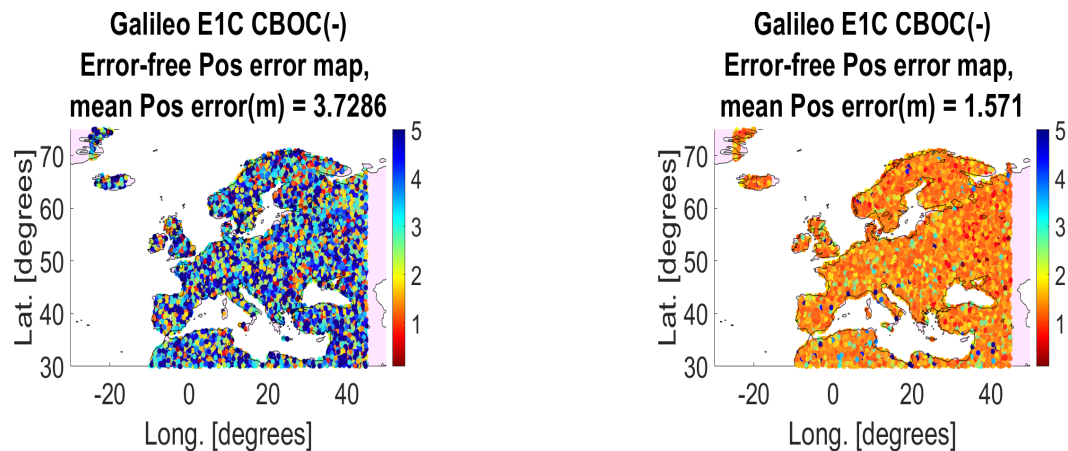
(c) Error-based positioning accuracy, Galileo E1C signal

(d) Error-free positioning accuracy, Galileo E1C signal

(e) Error-based positioning accuracy, terrestrial IoT (LoRa)

(f) Error-free positioning accuracy, terrestrial IoT (LoRa)

Fig. 7: Comparison of error-based position error (left plots) and error-free position error (right plots) for Starlink, Galileo, and terrestrial IoT system (LoRa).

based positioning," *EURASIP Journal on Advances in Signal Processing*, 01 2008.

[31] J. K. Ray, "Mitigation of gps code and carrier phase multipath effects using a multi-antenna system," 2000. [Online]. Available: https://prism.ucalgary.ca/handle/1880/42732

[32] A. J. VAN DIERENDONCK, P. FENTON, and T. FORD, "Theory and performance of narrow correlator spacing in a gps receiver," *NAVIGATION*, vol. 39, no. 3, pp. 265–283, 1992. [Online]. Available: https://onlinelibrary.wiley.com/doi/abs/10.1002/j.2161-4296.1992.tb02276.x

[33] J. Betz, "Design and performance of code tracking for the gps m code signal," in *Proceedings of ION-GPS*, 2000.
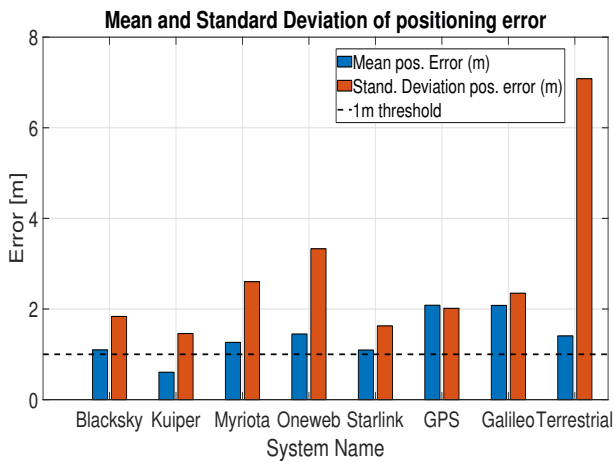
Fig. 8: Comparison of the mean and standard deviation of positioning error [m] for the eight systems under consideration.
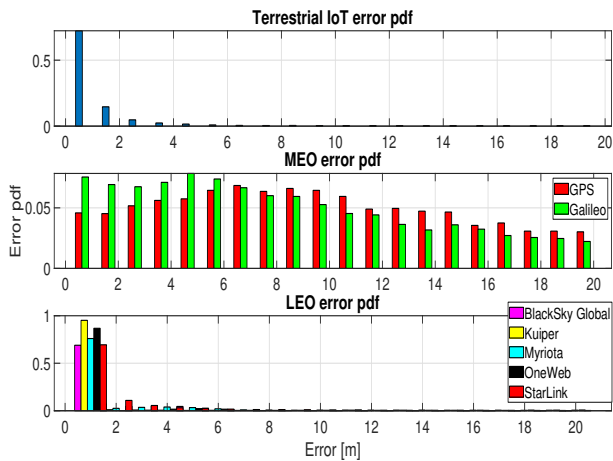

Fig. 9: Position error histogram distribution for the different constellations.

[34] J. W. Betz and K. R. Kolodziejski, "Extended theory of early-late code tracking for a bandlimited gps receiver," *NAVIGATION*, vol. 47, no. 3, pp. 211–226, 2000. [Online]. Available: https://onlinelibrary.wiley.com/doi/abs/10.1002/j.2161-4296.2000.tb00215.x

[35] A. Van Dierendonck, P. Fenton, and T. Ford, "Theory and performance of narrow correlator spacing in a gps receiver," *Navigation*, vol. 39, no. 3, pp. 265–283, 1992.

[36] N. Ziedan, *Global Navigation Satellite System (GNSS) Receivers for Weak Signals*. Artech, 2006.

[37] P. Teunissen and O. Montenbruck, *Springer handbook of global navigation satellite systems*. Springer, 2017.

[38] M. Chiani and A. Elzanaty, "On the lora modulation for iot: Waveform properties and spectral analysis," *IEEE Internet of Things Journal*, vol. 6, no. 5, pp. 8463–8470, 2019.

[39] K. Kuchi and V. K. Prabhu, "Power spectral density of gmsk modulation using matrix methods," in *MILCOM 1999. IEEE Military Communications. Conference Proceedings (Cat. No.99CH36341)*, vol. 1, 1999, pp. 45–50 vol.1.

[40] D. Vallado and W. McClain, *Fundamentals of Astrodynamics and Applications*, ser. Collège custom series. McGraw-Hill, 1997. [Online]. Available: https://books.google.fi/books?id=HuWMPwAACAAJ

[41] J. Prussing and B. Conway, *Orbital Mechanics*. Oxford University Press, 1993. [Online]. Available: https://books.google.fi/books?id=96xCER34THAC

R. Morales Ferre received both BSc in Telecommunication Systems Engineering and MSc in Telecommunication engineering from Universitat Autònoma de Barcelona (UAB) in 2016 and 2018, respectively. He is currently pursuing a double PhD degree in information and electrical engineering at Tampere University (TAU) and UAB. He worked as research assistant at UAB in Signal Processing for Communications & Navigation (SPCOMNAV) group until 2018. In 2018 he received a TAU rector's grant, which partially finances his PhD studies. He is also involved as a PhD researcher in EU funded projects such as GATEMAN, INNUENDO or NewSense and Academy of Finland funded projects such as ULTRA. His current research interests include GNSS security and integrity (GNSS jamming/spoofing interferences detection, classification, mitigation and localization), signal processing with applications to communications and navigation, and positioning by means of GNSS cellular networks such as 4G LTE or 5G systems, and array signal processing.

E.S. Lohan is a Professor at Tampere University (TAU), Finland. She received an M.Sc. degree in electrical engineering from Polytechnics University of Bucharest, Romania, in 1997, a D.E.A. degree (French equivalent of master) in econometrics at Ecole Polytechnique, Paris, France, in 1998, and a Ph.D. degree in telecommunications from Tampere University of Technology in 2003. She is now a professor at the Electrical Engineering unit at Tampere University, Finland and the coordinator of the MSCA EU A-WEAR network. Her current research interests include wireless location techniques, wearable computing, and privacy-aware positioning solutions